[1,2,3,4]Yansong Feng
[1,2,3]Xingming Wang
[1,2,3]Yuyang Liu
[1,2]Xue Bai
[1,2]Maoyou Chu
[1,2,3]Cheng Peng

Effect of YF_3 Coating Process on Film Stress

Abstract: - YF_3 rare-earth fluoride coating material has received wide attention as an alternative to ThF_4 low refractive index material, but the film layer can be seriously affected due to the different coating processes. Therefore, to investigate the rules between the coating processes of YF_3 rare-earth fluoride coating materials, YF_3 thin films were coated with different deposition rates and substrate temperatures. The stresses of YF_3 thin films under different processes were obtained by a thin film stress meter, and the microscopic morphology of the thin films was characterized by atomic force microscopy. The results show that: YF_3 monolayer film is tensile stress; in the deposition rate between 0.5nm/s~1.5nm/s, with the increase of the coating deposition rate YF_3 monolayer film stress tends to decrease, the roughness of the film is also gradually increased, and the overall thickness of the film surface decreases; in the substrate temperature is greater than 50 ℃, the film stress is significantly reduced.

Keywords: YF_3, Coating, Film Stress, Microscopic Morphology

INTRODUCTION

Optical components in infrared optical systems such as infrared detection, infrared measurement, infrared lasers, infrared imaging, infrared spectroscopy, etc. need to be coated with infrared thin films. The properties of infrared thin films required in different application contexts are also different [1-3].

Thorium fluoride (ThF_4) is an excellent infrared optical coating material with a refractive index of 1.35 at 10.6 μm and excellent mechanical properties, however, due to the presence of the radioactive element thorium, the search for its replacement has been the goal of optical thin-film material scientists around the world. With the development of thin-film technology and the wide application of rare earth, rare earth fluorides such as YF3 with a wide transparent region, lower refractive index, and strong bonding with the substrate material have become the preferred material to replace ThF_4.

For high-power laser systems, its optical thin film has a lower damage que value relative to other components, the laser damage threshold is often lower than the bare surface of the optical element 2 to 4 times [4], the development of optical thin film to date, the thin film damage mechanism has been systematic research, different damage mechanisms on the damage threshold of different impacts. Due to the lack of intuition about the damage mechanism, only discussing the damage mechanism can not comprehensively analyze the nature of the damage threshold, but also needs to be combined with the nature of thin film materials and laser parameters to further develop the study. Moreover, different thin film materials have their unique physicochemical properties, and different preparation processes and methods will also cause different results. For the same material and the same preparation process, the laser damage of the thin film will also show obvious differences with different processes.

Therefore, the anti-laser strength of the optical thin film is an important basis for the design of laser systems and the maximum limit, improving the performance of the thin film, and improving its damage threshold has more important practical significance, because of this, the performance of optical thin film will directly affect the performance index of the laser system. For this reason, many international thin film and laser engineering laboratories have invested a lot of manpower and material resources to carry out the research work in this area

*Corresponding author: Xingming Wang,1454524376@qq.com
[1]National Engineering Research Center for Environment-friendly Metallurgy in Producing Premium Non-ferrous Metals, GRINM Group Corporation Limited, Beijing100088, China;
[2]GRINM Resources and Environment Tech. Co. Ltd., Beijing100088, China
[3]General Research Institute for Nonferrous Metals, Beijing 100088, China
[4]Beijing Engineering Research Center of Strategic Nonferrous Metals Green Manufacturing Technology, Beijing 100088, China
Copyright © JES 2024 on-line : journal.esrgroups.org

one after another. The anti-laser damage threshold is closely related to the film stress, to a large extent, the size of the film stress will seriously affect the anti-laser damage threshold.

The coating process [5-8] involves the coating process and various process parameters, the selection and treatment of substrate materials, aging treatment, post-treatment, and other factors. Among them, the substrate temperature and deposition rate, as the main influences of the coating process, are particularly important to the quality of the film.

To address the above problems, this study takes rare earth fluoride coating material YF3 as the research object, and uses vacuum physical deposition to coat YF_3 thin films, expecting to explore the suitable coating process, to find out the influence of the coating process on the film stress, and to carry out AFM characterization of YF_3 thin films of low refractive index materials, to explore the mechanism of the growth of YF_3 thin films.

I MATERIALS AND METHODS

To investigate the effect of deposition rate on the stress of yttrium fluoride monolayer films, YF_3 monolayer films were deposited in this thesis on (φ50mm×5mm) single crystal silicon samples polished on both sides with different deposition rates. The vacuum during film deposition was 5×10^{-3} Pa, and the deposition rate and film thickness were monitored by a quartz crystal oscillator. Yttrium fluoride films were deposited by electron beam heating with a film thickness of about 1400 nm, and the deposition rates ranged from 5, 10, and 15 A/s, respectively, with substrate temperatures of 50 °C, 100 °C, 150 °C, and 200 °C.

II RESULTS

In this experiment, the height of the sample surface was directly obtained by AFM testing the magnitude of the interaction force between atoms, and the image was plotted to obtain information on the surface topography of the film, which fully demonstrated the roughness and topography of the film surface. The changes in the surface shape of the YF_3 film were measured by a thin film stress meter and the stresses in the four directions of 0, 45°, 90°, and 135° were calculated.

A Effect of deposition rate on film stress

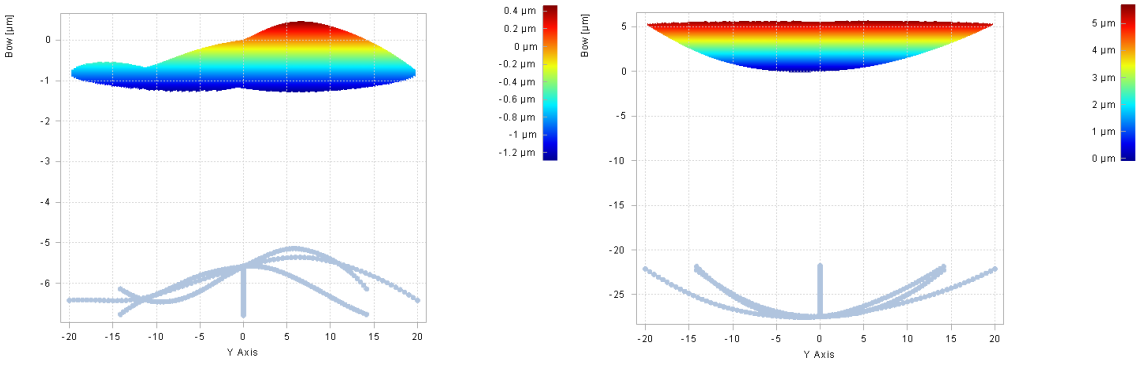

Figure 3.1 Stress surface pattern at a deposition rate of 0.5 nm/s: (left) before coating (right) after coating

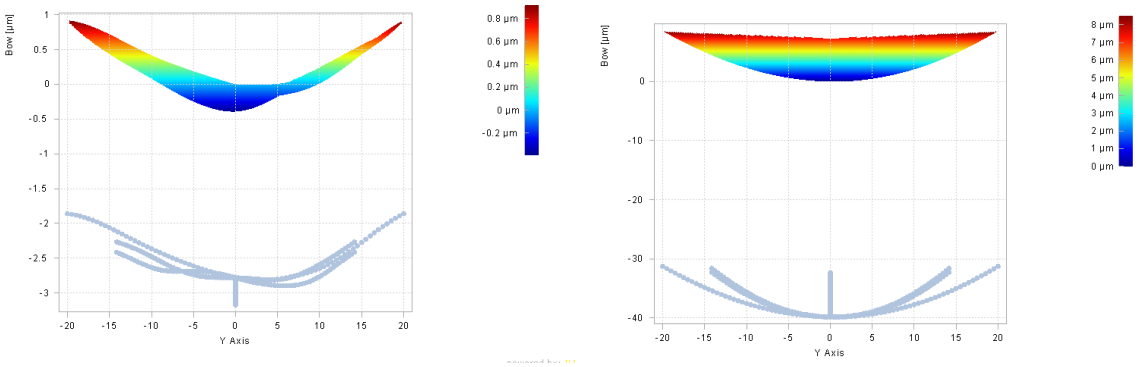

Figure 3.2 Stress surface pattern at a deposition rate of 1.0 nm/s: (left) before coating (right) after coating

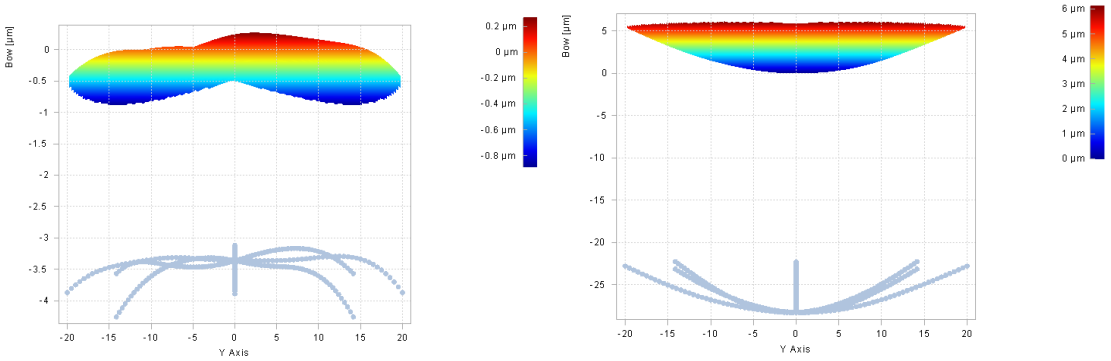

Figure 3.3 Stress surface pattern at a deposition rate of 1.5 nm/s: (left) before coating (right) after coating

From Figures 3.1, 3.2, and 3.3, it can be found that the stress surface patterns at all three deposition rates are upward stretching stresses, indicating that the stresses in the films are tensile stresses and contraction of the films concerning the substrate surface.

By geometry and mechanics, it can be inferred that the change in surface curvature of the thin film sample will affect the stress. The radius of curvature of the sample (substrate) before coating is set to be R0, and the radius of curvature after coating is set to be R1. When the thickness ts of the sample (the film is so thin that the thickness of the substrate can be regarded as the thickness of the sample) is much less than R1, then the stresses in the film can be calculated using Stoney's formula.

$$\sigma = \frac{E_s t_s^2}{6(1-\nu_s)t_f}\left(\frac{1}{R_1}-\frac{1}{R_0}\right) \qquad (3.1)$$

Where: Es is the Young's modulus of the substrate, take 82 GPa; Vs is the Poisson's ratio of the substrate, take 0.206; ts is the thickness of the sample, take 2 mm; tf is the thickness of the film, 1.4 μm.

For the three deposition rates of the film in four directions, 0°, 45°, 90°, and 135°, Stoney's formula as in Eq. 3.1 was used to calculate the stresses as follows.

Table 3.1 Details of four-directional surface stresses in films at a deposition rate of 0.5 nm/s

angles	lengths (mm)	curvature (1/m)	curvature radius (m)	Bow(μm)	Warp(μm)	stress value (MPa)
0°	40.0	$3.741*10^{-2}$	26.733	-7.5	7.5	201.01
45°	40.0	$3.777*10^{-2}$	26.477	-7.6	7.6	202.96
90°	40.0	$3.816*10^{-2}$	26.203	-7.6	7.6	205.08
135°	40.0	$3.689*10^{-2}$	27.106	7.4	7.4	198.25

Table 3.2 Details of four-directional surface stresses in films at a deposition rate of 1.0 nm/s

angles	lengths (mm)	curvature (1/m)	curvature radius (m)	Bow(μm)	Warp(μm)	stress value (MPa)
0°	40.0	$3.027*10^{-2}$	33.034	-6.1	6.1	162.67
45°	40.0	$3.109*10^{-2}$	32.161	-6.2	6.2	167.09
90°	40.0	$3.265*10^{-2}$	30.627	-6.5	6.5	175.46
135°	40.0	$2.997*10^{-2}$	33.370	-6.0	6.0	161.03

Table 3.3 Details of four-directional surface stresses in films at a deposition rate of 1.5 nm/s

angles	lengths (mm)	curvature (1/m)	curvature radius (m)	Bow(μm)	Warp(μm)	stress value (MPa)
0°	40.0	$3.077*10^{-2}$	32.497	-6.2	6.2	165.36
45°	40.0	$3.206*10^{-2}$	31.194	-6.4	6.4	172.27
90°	40.0	$3.440*10^{-2}$	29.069	-6.9	6.9	184.86
135°	40.0	$3.077*10^{-2}$	32.494	-6.2	6.2	165.37

From Table 3.1, 3.2, 3.3, it can be seen that the YF_3 monolayer film three deposition rate of the four directions of the stress is tensile stress, indicating that the uniformity of the film is better, and with the increase of the deposition rate of the film stress is a tendency to reduce, and the directional surface of the film in the direction of 0 °, 135 ° direction than the 45 °, 90 ° direction of the film stress is smaller, may be due to the non-circular contour of the substrate 0 °, 135 ° between the result of the noncircularity of the contour.

From Figures 3.4, 3.5, and 3.6 AFM it can be seen that as the coating deposition rate increases the roughness of the film increases gradually, the deposition rate of 0.5nm/s and 1.0nm/s surface roughness root mean square is 1.42nm, as the deposition rate increases to 1.5nm/s the film surface roughness root mean square increases to 2.06nm.

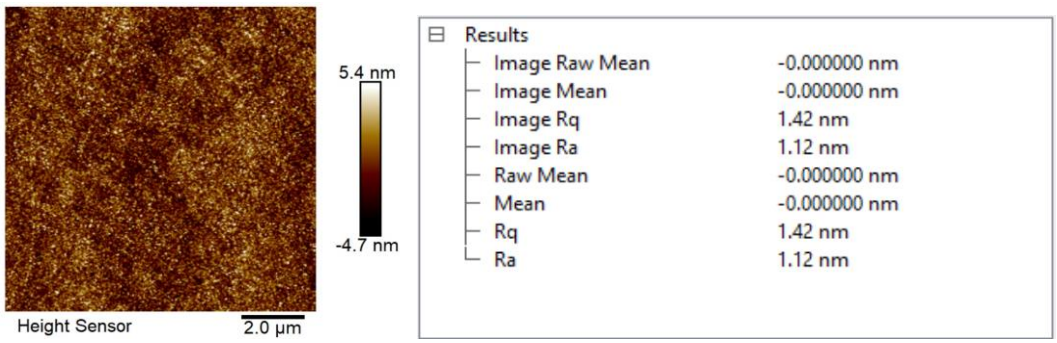

Figure 3.4 AFM at a deposition rate of 0.5 nm/s

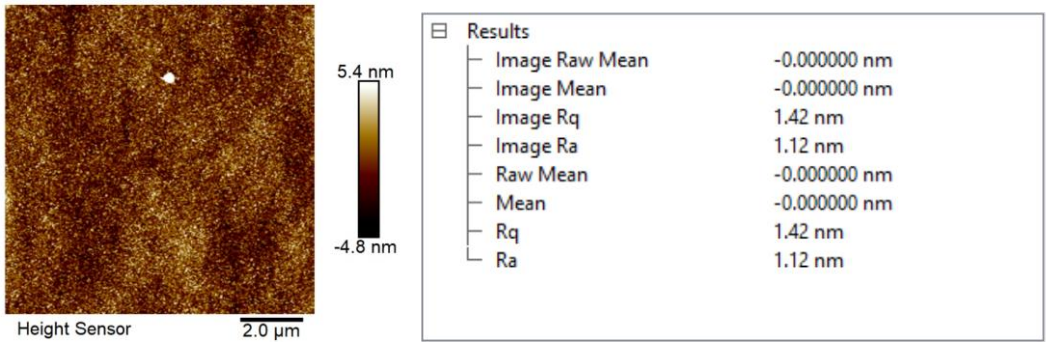

Figure 3.5 AFM at a deposition rate of 1.0 nm/s

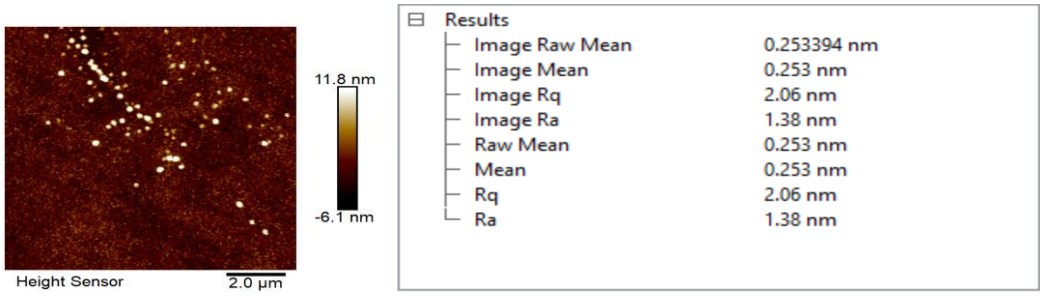

Figure 3.6 AFM at a deposition rate of 1.5 nm/s

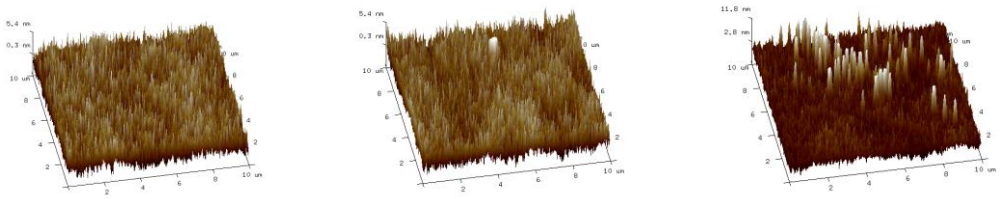

Figure 3.7 3d morphology of films with different deposition rates (0.5 nm/s on the left 1.0 nm/s in the middle 1.5 nm/s on the right)

From Figure 3.7 3D stereograms of the coating at three rates, it can be seen that the surface morphology of the YF3 monolayer film showed many peaks or needle-like bumps, the height of the surface bumps between 0.3~5.4 nm, while the local surface morphology of the YF3 monolayer film is no difference in the vertical direction, and the white bumps are the particles adhering to the film surface, and it can be seen that with the increase in the rate of deposition of the film surface attached to the increase in the number of particles. It can be seen that with the increase of deposition rate, the film surface attached particles increase, probably due to the high deposition rate, and too much introduction of impurities into the vacuum chamber into the film (have been wiped before the test).

B Influence of substrate temperature on film stresses

In the previous section, the effect of deposition rate on yttrium fluoride monolayer stress was investigated, and 1.0 nm/s was selected as the YF_3 coating rate. This section continues to explore the effect of substrate temperature on yttrium fluoride monolayer stress. The YF_3 monolayer film was deposited on a double-sided polished single-crystal silicon sample (φ50mm×5mm) at a deposition rate of 1.0nm/s after melt crystallization at 1400°C for 2h. The vacuum during film deposition was better than that of the YF_3 monolayer film. The vacuum during film deposition was better than 8×10^{-3}pa, and the deposition rate and film thickness were monitored by a quartz crystal oscillator. Yttrium fluoride films were deposited by electron beam heating, with a film thickness of about 1400 nm, and the substrate temperatures for deposition were selected as 50°C, 100°C, 150°C, and 200°C, respectively. The average radius of curvature of the double-sided polished Si wafer substrate before coating was obtained, which was used to calculate the film stress by subsequent calculation of the change in radius of curvature after coating.

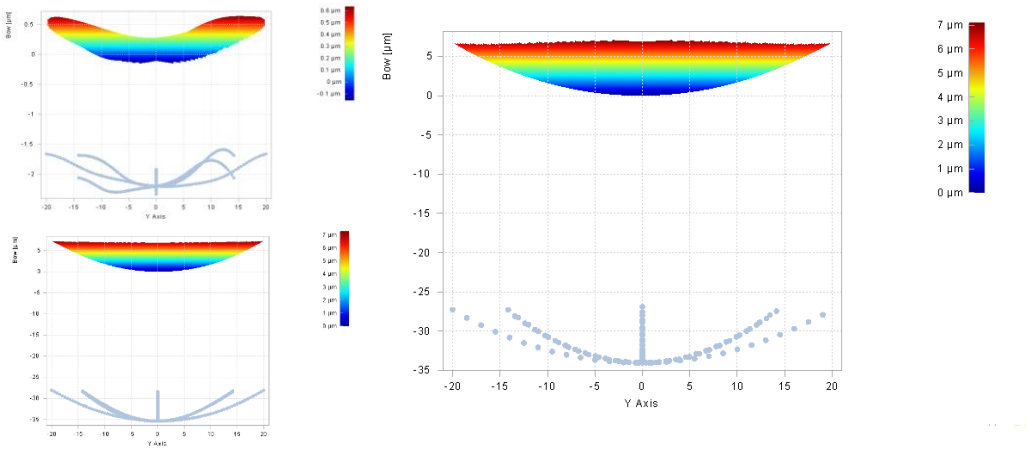

Figure 3.8 Stress surface pattern at 50°C substrate temperature: (top left) substrate (bottom left) coating (right) vs. reduced

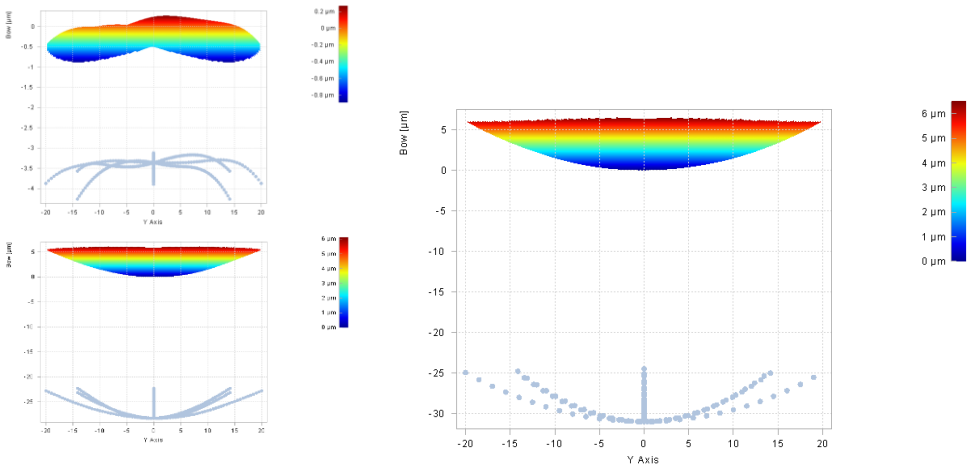

Figure 3.9 Stress surface pattern for substrate temperature 100°C: (top left) substrate (bottom left) coating (right) vs. Reduced

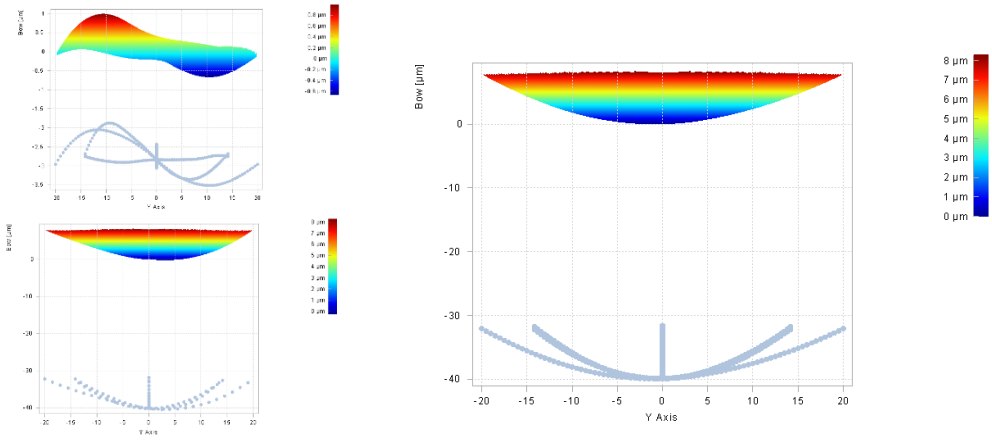

Figure 3.10 Stress surface pattern for substrate temperature 150°C: (top left) substrate (bottom left) coating (right) vs. reduced

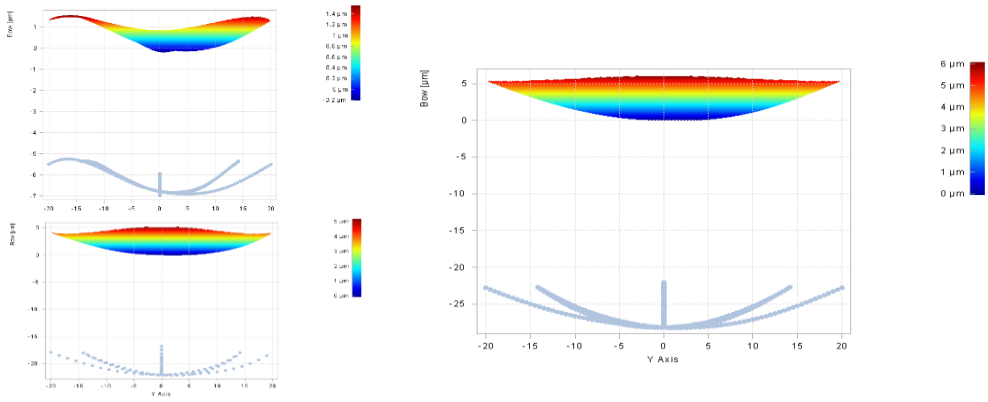

Figure 3.11 Stress surface pattern for substrate temperature 200°C: (top left) substrate (bottom left) coating (right) vs. reduced

From Figure 3.8-3.11 four substrate temperature film stress patterns can be seen, the y-axis direction of the film stress pattern is both ends upward pull-up pattern that is, the film relative to the substrate surface contraction is tensile stress.

For the four substrate temperature plated film four directions face 0 °, 45 °, 90 °, and 135 ° using the Stoney formula as in equation 3.1 for the stress calculation results are as follows.

Table 3.4 Details of four-directional surface stresses in films at 50°C substrate temperature

angles	lengths (mm)	curvature (1/m)	curvature radius (m)	Bow(μm)	Warp(μm)	stress value (MPa)
0°	40.0	$3.950*10^{-2}$	25.315	-7.9	7.9	212.28
45°	40.0	$4.031*10^{-2}$	24.806	-8.1	8.1	216.63
90°	40.0	$4.280*10^{-2}$	23.364	-8.6	8.6	230.00
135°	40.0	$4.055*10^{-2}$	24.660	-8.1	8.1	217.91

Table 3.5 Details of four-directional surface stresses in films at a substrate temperature of 100°C

angles	lengths (mm)	curvature (1/m)	curvature radius (m)	Bow(μm)	Warp(μm)	stress value (MPa)
0°	40.0	$3.626*10^{-2}$	27.578	-7.3	7.3	194.85
45°	40.0	$3.561*10^{-2}$	28.080	-7.1	7.1	191.37
90°	40.0	$3.797*10^{-2}$	26.337	-7.6	7.6	204.04
135°	40.0	$3.504*10^{-2}$	28.538	-7.0	7.0	188. 3

Table 3.6 Details of four-directional surface stresses in films at a substrate temperature of 150°C

angles	lengths (mm)	curvature (1/m)	curvature radius (m)	Bow(μm)	Warp(μm)	stress value (MPa)
0°	40.0	$4.093*10^{-2}$	24.429	-8.2	8.2	219.97
45°	40.0	$4.061*10^{-2}$	24.627	-8.1	8.1	218.20
90°	40.0	$4.145*10^{-2}$	24.124	-8.3	8.3	222.75
135°	40.0	$3.786*10^{-2}$	26.416	-7.6	7.6	203.42

Table 3.7 Details of four-directional surface stresses in films at a substrate temperature of 200°C

angles	lengths (mm)	curvature (1/m)	curvature radius (m)	Bow(μm)	Warp(μm)	stress value (MPa)
0°	40.0	3.378*10-2	29.600	-6.8	6.8	181.54
45°	40.0	3.379*10-2	29.597	-6.8	6.8	181.56
90°	40.0	3.561*10-2	28.084	-7.1	7.1	191.34
135°	40.0	3.293*10-2	30.368	-6.6	6.6	176.95

As can be seen from Table 3.4-3.7, the stress of YF_3 single-layer film is tensile stress, and the film stress fluctuates irregularly with the increase of the base temperature, in which the film stress decreases first, then increases, and then decreases. When the base temperature is 200℃, the film stress is the lowest at 110Mpa. The film stress in the direction of 0°, 45°, and 135° is generally smaller than that in the direction of 90°, which may be caused by the non-circular contour between the substrates.

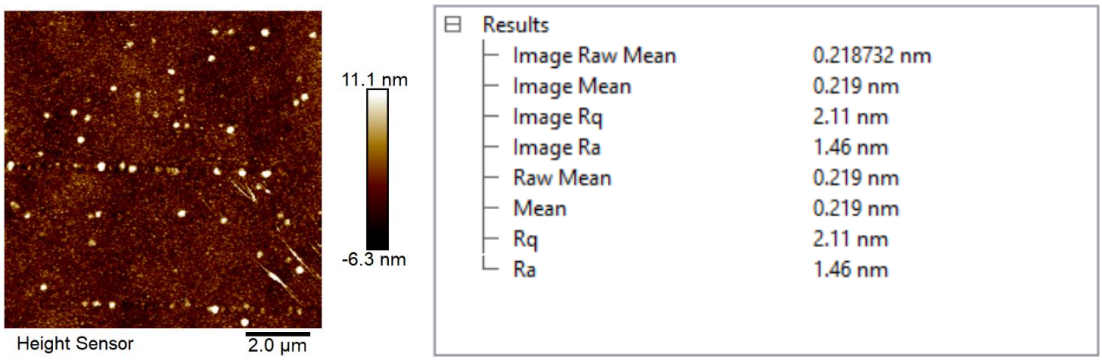

Figure 3.12 AFM plot at 50°C substrate temperature

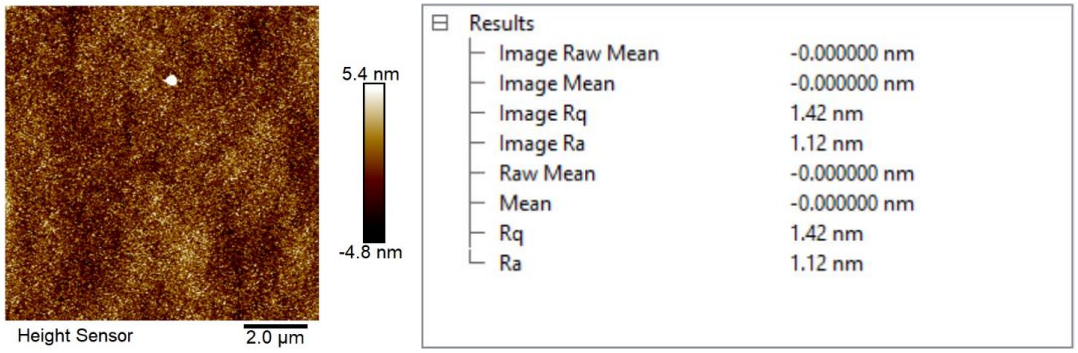

Figure 3.13 AFM plot at 100°C substrate temperature

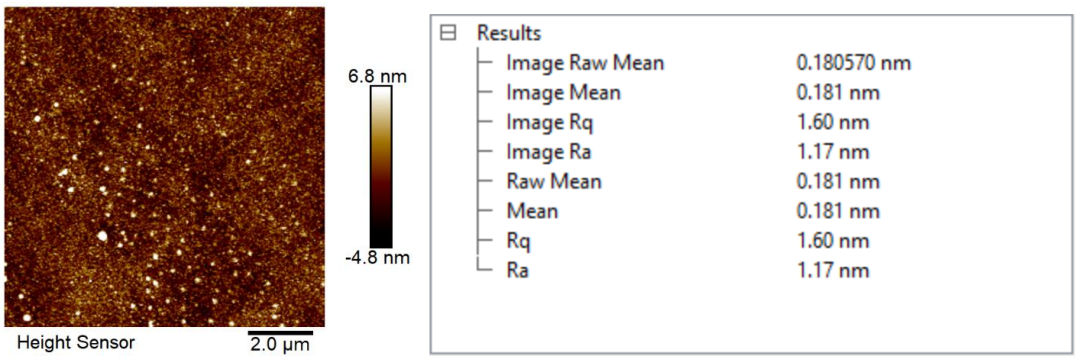

Figure 3.14 AFM plot at 150°C substrate temperature

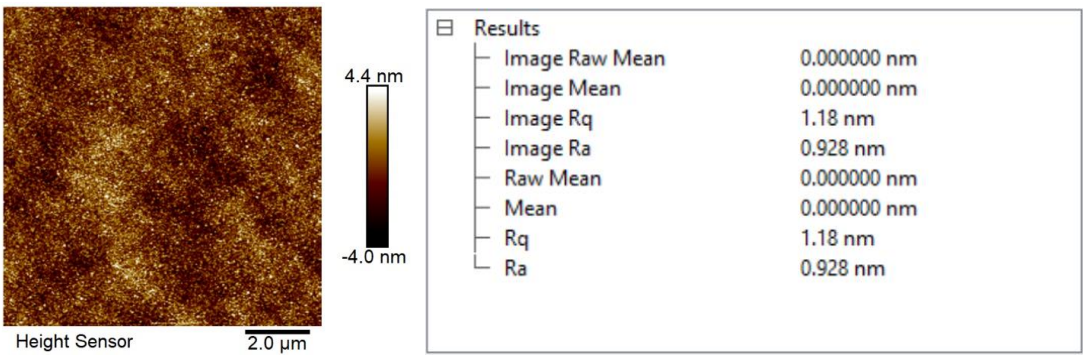

Figure 3.15 AFM plot at 200°C substrate temperature

From Figure 3.12-3.17 it can be seen that with the increase of the coating substrate temperature of the film

roughness of the root mean square is gradually reduced, the substrate temperature of 50 ℃ surface roughness root mean square is 2.11 nm, 100 ℃ for 1.42 nm, 150 ℃ for 1.60 nm, 200 ℃ for 1.18 nm. the average roughness of the surface of the film temperature of 50 ℃ is 1.12 nm, 100 ℃ for 1.17 nm, and 150° C is 0.928 nm, which indicates that the roughness of the film gradually decreases and then fluctuates as the substrate temperature increases.

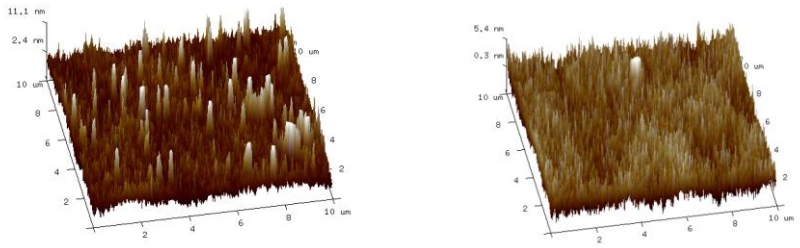

Figure 3.16 Thin film morphology corresponding to different substrate temperatures (left: 50°C right: 100°C)

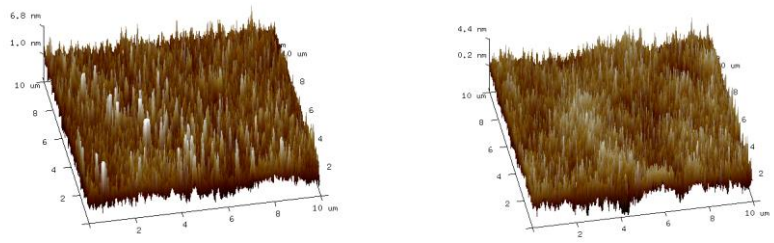

Figure 3.17 Thin film morphology corresponding to different substrate temperatures (left: 150°C right: 200°C)

III DISCUSSION

The morphology of the films plated at the four substrate temperatures shows that the increase in substrate temperature affects the morphology of the films, with the increase in substrate temperature the overall thickness of the film surface decreases, and the peak-like inhomogeneous distribution is gradually aggravated. When the substrate temperature is low, the atoms cannot have enough thermal energy to migrate to the corresponding positions on the substrate due to insufficient thermal energy, thus randomly forming multiple nucleation sites. These nucleation sites grow slowly to form peaks, which continue to grow to form a film with a certain thickness.

IV CONCLUSIONS

In this study, the vacuum evaporation coating of YF_3 coating material was used as a means to investigate the effects of deposition rate, substrate temperature, and other coating processes on the film properties, and the main conclusions are as follows.

(1) The YF_3 monolayer film coated on a double-sided polished silicon wafer shrinks relative to the substrate surface, and the film stress is tensile; due to the non-circular contour between the substrates, the film stress in the 0 °, 45 °, and 135 ° directions is generally smaller than that in the 90 ° direction.

(2) In the deposition rate of 0.5nm / s ~ 1.5nm / s, with the increase in the deposition rate of the coating YF_3 monolayer film stress tends to decrease, the roughness of the film is also gradually increased, the overall

thickness of the film surface is reduced; in the substrate temperature is greater than 50 ℃ film stress is significantly reduced.

REFERENCES

[1] Ning B, Wu Y. Research on Non-contact Infrared Temperature Measurement[J]. Sensor World, 2001, 30(1):1-4.

[2] Lahiri B B, Bagavathiappan S, Jayakumar T, et al. Medical applications of infrared thermography: A review[J]. Infrared Physics & Technology, 2012, 55(4): 221-235.

[3] Eklund S E, Toth L M, Chambers J Q, et al. Determination of oxide in fluoride salts using a yttria-stabilized-zirconia oxygen pump[J]. Analytical chemistry, 1999, 71(3): 539-43.

[4] Stuart BC, Feit MD, Rubenchik A M, et al.Laser-induced damage in dielectrics with nanosecond to subpicosecond pulses.[J]. Physical Review Letters, 1994, 74(12):2248-2251.

[5] Soref R. Mid-infrared photonics in silicon and germanium[J]. Nature Photonics, 2010, 4: 495-497.

[6] Titterton D H. Development of infrared countermeasure technology and systems[J]. Springer, 2006, 118:635-671.

[7] Younus A M D, Yang B-S. Intelligent fault diagnosis of rotating machinery using infrared thermal image[J]. Expert Systems with Applications, 2012, 39(2): 2082-2091.

[8] Siciliani De Cumis M, Viciani S, Borri S, et al. Widely-tunable mid-infrared fiber-coupled quartz-enhanced photoacoustic sensor for environmental monitoring[J]. Optics Express, 2014, 22(23): 28222-28231.